Full-Wave Model of Frequency-Dispersive Media With Debye Dispersion Relation by Circuit-Oriented FEM

Francescaromana Maradei, *Senior Member, IEEE*, Haixin Ke, *Member, IEEE*, and Todd H. Hubing, *Fellow, IEEE*

***Abstract*—Dispersive materials play an important role in a wide variety of applications (e.g., waveguides, antenna structures, integrated circuits, bioelectromagnetic applications). In this paper, a full-wave finite-element method (FEM-SPICE) technique for modeling dispersive materials is proposed. A finite-element formulation employing Whitney elements capable of analyzing electromagnetic geometries with dispersive media is described, and a Norton equivalent network is developed for each element. The overall network can be analyzed using a circuit simulator based on SPICE, and is suitable for both frequency- and time-domain analysis. This approach exploits the flexibility of finite-element mesh generation and computational efficiency of modern circuit simulators. Simple test configurations are analyzed to validate the proposed formulation.**

***Index Terms*—Biological applications, circuit analysis, Debye model, dispersive media, finite-element method (FEM), integrated circuits (ICs), SPICE circuit simulator, Whitney element.**

I. Introduction

THE ABILITY to analyze electromagnetic problems that include frequency-dispersive materials is increasingly important as these materials are found in a growing number of applications. Biological tissue is an important class of dispersive media and is involved in studies of dosimetry to assess human exposure to radio-frequency (RF) and microwave (MW) radiation, in therapeutic applications of electromagnetic (EM) fields such as treating hyperthermia, and in several diagnostic applications of EM fields to detect the possible presence of tumors [1], [2]. Another class of dispersive media is represented by the dielectric materials used in integrated circuits (ICs), antenna structures, and waveguides [3]–[5]. In particular, when analyzing digital signal propagation at very high data rates, accurate modeling of the dispersion is of paramount importance.

In recent years, the analysis of field propagation in structures containing frequency-dispersive media has been mainly performed using the finite-difference time-domain (FDTD) method [6]–[9]. Although the standard FDTD method is not well suited for modeling curved surfaces or complex configurations with significant variations in scale, it is the most widely used time-domain numerical method largely due to the simplicity of the solution algorithm.

The Whitney-element time-domain (WETD) method has been recently extended to model dispersive materials [10]–[12]. The WETD method is an implicit method suitable for the analysis of complex configurations. WETD is characterized by its superior mesh flexibility, but it is more time-consuming on a per-element basis than FDTD.

In the past decade, significant progress has been made in the development of numerical tools suitable for analyzing field-circuit coupled problems [13]–[26]. This class of problems is relevant to the design of electrical/electronic devices and in electromagnetic compatibility (EMC) applications. In particular, several circuit-oriented techniques based on the finite-element method (FEM) have been developed [20]–[26]. These techniques combine the flexible mesh generation and analysis capabilities of FEM methods for solving full-wave EM equations, with the fast solution capabilities of optimized circuit solvers. The main advantage of circuit-oriented FEM is the capability to exploit the ability of SPICE-like simulators to model linear/nonlinear components embedded in distributed EM geometries.

The aim of this paper is to extend the circuit-oriented FEM formulation proposed in [25] and improved in [26], to account for frequency-dispersive media. In the proposed approach, a Norton equivalent network corresponding to the field domain is derived from the edge element solution of the vector wave equation for dispersive media. Each edge of the FEM mesh is modeled as a port of an electrical network, which is coupled with other ports (i.e., edges) through the equivalent admittance matrix. Circuit components embedded in the field domain can be directly introduced in the equivalent electrical network, and the resulting network can be readily analyzed in either the time or frequency domain using a SPICE circuit simulator.

In Section II, a Whitney element formulation for frequency-dispersive materials characterized by Debye function expansion is proposed, and the derivation of the corresponding Norton equivalent network is discussed. In Section III, this formulation is extended to account for media characterized by multiple relaxation processes and a multiterm Debye model is developed [8], [27]. Numerical examples are provided in Section IV to validate the proposed formulation, and conclusions are drawn in Section V.

Manuscript received June 13, 2008; revised November 28, 2008. First published April 10, 2009; current version published May 15, 2009.

F. Maradei is with the Department of Electrical Engineering, Sapienza University, 00184 Rome, Italy (e-mail: francesca.maradei@uniroma1.it).

H. Ke and T. H. Hubing are with the Department of Electrical and Computer Engineering, Clemson University, Clemson, SC 29634 USA (e-mail: hxkeucl@clemson.edu; hubing@exchange.clemson.edu).

Color versions of one or more of the figures in this paper are available online at http://ieeexplore.ieee.org.

Digital Object Identifier 10.1109/TEMC.2009.2014639

II. Mathematical Formulation

A. Electric Field Wave Equation for Dispersive Media

Electromagnetic fields in the frequency domain can be described by Maxwell's curl equations

$$\nabla \times \boldsymbol{E} = -j\omega\mu\boldsymbol{H} \tag{1a}$$

$$\nabla \times \boldsymbol{H} = \boldsymbol{J}_{\mathrm{s}} + j\omega\boldsymbol{D} \tag{1b}$$

where $\boldsymbol{E}$ and $\boldsymbol{H}$ are the time-harmonic electric and magnetic field vectors, respectively, $\boldsymbol{J}_{\mathrm{s}}$ is the current density of an impressed source, $\boldsymbol{D}$ is the electric flux density, ω is the angular frequency, and μ is the permeability of the medium.

The constitutive relation for a medium characterized by a frequency-dependent permittivity is

$$\boldsymbol{D} = \varepsilon_0 \hat{\varepsilon}_{\mathrm{r}}(\omega)\boldsymbol{E} \tag{2}$$

where ε_0 is the permittivity of free space and $\hat{\varepsilon}_{\mathrm{r}}(\omega)$ is the complex relative permittivity given by

$$\hat{\varepsilon}_{\mathrm{r}}(\omega) = \varepsilon_{\mathrm{r}}(\omega) - j\frac{\sigma(\omega)}{\omega\varepsilon_0} = \varepsilon_\infty - j\frac{\sigma_0}{\omega\varepsilon_0} + \chi(\omega) \tag{3}$$

where $\varepsilon_{\mathrm{r}}(\omega)$ and $\sigma(\omega)$ are the frequency-dependent relative permittivity and conductivity, respectively, ε_∞ is the permittivity as $\omega \to \infty$, σ_0 is the conductivity as $\omega \to 0$, and $\chi(\omega)$ is the electric susceptibility. For a medium with a Debye dispersion relation, the electric susceptibility is given by [6]–[9]

$$\chi(\omega) = \frac{\varepsilon_{\mathrm{s}} - \varepsilon_\infty}{1 + j\omega\tau_0} \tag{4}$$

where ε_{s} is the static permittivity and τ_0 the relaxation time.

The frequency domain vector wave equation in terms of the electric field $\boldsymbol{E}$ can be obtained via (1) and (2) as

$$\nabla \times \frac{1}{j\omega\mu}\nabla \times \boldsymbol{E} + \sigma_0\boldsymbol{E} + j\omega\varepsilon_0[\varepsilon_\infty + \chi(\omega)]\boldsymbol{E} = -\boldsymbol{J}_{\mathrm{s}}. \tag{5}$$

B. Whitney Element Formulation

For any complex computational domain Ω bounded by a closed surface Γ as shown in Fig. 1, the Galerkin form of (5) is given by [28]

$$\int_\Omega \frac{1}{j\omega\mu}(\nabla \times \mathbf{u}) \cdot (\nabla \times \boldsymbol{E})\mathrm{d}\Omega + \int_\Omega \sigma_0 \mathbf{u} \cdot \boldsymbol{E}\mathrm{d}\Omega + \int_\Omega \mathrm{j}\omega\varepsilon_0[\varepsilon_\infty + \chi(\omega)]\mathbf{u} \cdot \boldsymbol{E}\,\mathrm{d}\Omega + \int_\Omega \mathbf{u} \cdot \boldsymbol{J}_{\mathrm{s}}\,\mathrm{d}\Omega - \int_\Gamma \frac{1}{\mathrm{j}\omega\mu}(\mathbf{u} \times \nabla \times E) \cdot \hat{\mathbf{n}}\mathrm{d}\Gamma = 0 \tag{6}$$

where $\mathbf{u}$ is the vector weighting function and $\hat{\mathbf{n}}$ is the outward unit vector normal to the boundary Γ. For simplicity, the contribution of the boundary integral is not taken into account here. The implementation of different boundary conditions is described in [28].

Equation (6) can be solved by applying the FEM using Whitney elements. The computational domain is discretized into N_{T} arbitrarily shaped finite elements $\Omega^{(\mathrm{e})}$ so that $\Omega = \Sigma_{\mathrm{e}}\Omega^{(\mathrm{e})}$ with $\mathrm{e} = 1, N_{\mathrm{T}}$. The mesh is defined by N_{N} nodes and N_{E} edges. The

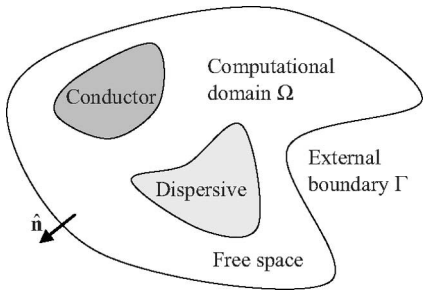

Fig. 1. Complex computational domain Ω bounded by a closed surface Γ.

electric field vector $\boldsymbol{E}$ is locally approximated by the Whitney 1-form [10], [28]

$$\boldsymbol{E}(\mathbf{r}) \cong \sum_{k=1}^{n} \mathbf{w}_k(\mathbf{r})e_k \tag{7}$$

where $\mathbf{r}$ is the position vector, n is the number of element edges in a given element $\Omega^{(\mathrm{e})}$, $\mathbf{w}_k(\mathbf{r})$ is the vector trial function associated with the kth edge, and e_k is the circulation of the electric field along the kth edge defined as

$$e_k = \int_{\lambda_k} \boldsymbol{E} \cdot \hat{\boldsymbol{t}}_k \mathrm{d}\ell \tag{8}$$

where $\hat{\boldsymbol{t}}_k$ is the kth edge tangent unit vector and λ_k the kth edge length. Substituting (7) into (6), and assuming $\mathbf{u} = \mathbf{w}_k$, with $k = 1, 2, \ldots, n$, the following local equation system is obtained:

$$\frac{[S^{(\mathrm{e})}]}{j\omega\mu^{(\mathrm{e})}}[e^{(\mathrm{e})}] + \sigma_0^{(\mathrm{e})}[T^{(\mathrm{e})}][e^{(\mathrm{e})}] + j\omega\varepsilon_0(\varepsilon_\infty^{(\mathrm{e})} + \chi^{(\mathrm{e})}(\omega))[T^{(\mathrm{e})}][e^{(\mathrm{e})}] = -[I_{\mathrm{S}}^{(\mathrm{e})}] \tag{9}$$

where $\mu^{(\mathrm{e})}$, $\sigma_0^{(\mathrm{e})}$, $\varepsilon_\infty^{(\mathrm{e})}$, and $\chi^{(\mathrm{e})}(\omega)$ are the medium-specific constants of the given homogeneous finite element $\Omega^{(\mathrm{e})}$, $[e^{(\mathrm{e})}] = [e_1^{(\mathrm{e})} e_2^{(\mathrm{e})} \ldots e_n^{(\mathrm{e})}]^{\mathrm{t}}$ is the vector of the electric field circulation along the element edges, $[S^{(\mathrm{e})}]$ and $[T^{(\mathrm{e})}]$ are the element stiffness and mass matrices, respectively, and $[I_{\mathrm{S}}^{(\mathrm{e})}]$ is the element source current vector. The coefficients of $[S^{(\mathrm{e})}]$, $[T^{(\mathrm{e})}]$, and $[I_{\mathrm{S}}^{(\mathrm{e})}]$ are given by

$$S_{i,j}^{(\mathrm{e})} = \int_{\Omega^{(\mathrm{e})}} \nabla \times \mathbf{w}_i \cdot \nabla \times \mathbf{w}_j \mathrm{d}\Omega \tag{10a}$$

$$T_{i,j}^{(\mathrm{e})} = \int_{\Omega^{(\mathrm{e})}} \mathbf{w}_i \cdot \mathbf{w}_j \mathrm{d}\Omega \tag{10b}$$

$$I_{\mathrm{si}}^{(\mathrm{e})} = \int_{\Omega^{(\mathrm{e})}} \mathbf{w}_i \cdot \boldsymbol{J}_{\mathrm{s}}\,\mathrm{d}\Omega. \tag{10c}$$

It should be noted that (10c) is nonzero only when $\boldsymbol{J}_{\mathrm{s}}$ is nonzero in a given finite element $\Omega^{(\mathrm{e})}$.

The assembly procedure for the local system of (9) yields the global system

$$\frac{[S_\mu]}{j\omega}[e] + [T_\sigma][e] + j\omega[T_\varepsilon][e] + j\omega[T_\chi(\omega)][e] = -[I_{\mathrm{S}}] \tag{11}$$

where $[e] = [e_1 e_2 \cdots e_{N_{\mathrm{E}}}]^{\mathrm{t}}$ is the global vector of the electric field circulations, and $[I_{\mathrm{S}}]$ is the global source current

vector obtained by assembling the local vectors $[I_{\rm S}^{(\rm e)}]$ (i.e., $[I_{\rm S}] = \Sigma_{\rm e}[I_{\rm S}^{(\rm e)}]$). $[S_\mu]$, $[T_\sigma]$, $[T_\varepsilon]$, and $[T_\chi(\omega)]$ are the global matrices obtained by assembling the local elemental matrices as

$$[S_\mu] = \sum\nolimits_{\rm e} \frac{1}{\mu^{(\rm e)}}[S^{(\rm e)}] \tag{12a}$$

$$[T_\sigma] = \sum\nolimits_{\rm e} \sigma_0^{(\rm e)}[T^{(\rm e)}] \tag{12b}$$

$$[T_\varepsilon] = \sum\nolimits_{\rm e} \varepsilon_0 \varepsilon_\infty^{(\rm e)}[T^{(\rm e)}] \tag{12c}$$

$$[T_\chi(\omega)] = \sum\nolimits_{\rm e} \varepsilon_0 \chi^{(\rm e)}(\omega)[T^{(\rm e)}] \tag{12d}$$

where the symbol $\Sigma_{\rm e}$ refers to the assembling operator.

The global system (11) can be rewritten in compact form as

$$[Y_{\rm WE}(\omega)][e] = -[I_{\rm S}] \tag{13}$$

where $[Y_{\rm WE}(\omega)]$ is a nonsingular sparse symmetric square matrix, whose coefficients are given by

$$Y_{{\rm WE}_{i,j}}(\omega) = \frac{S_{\mu_{i,j}}}{j\omega} + T_{\sigma_{i,j}} + j\omega T_{\varepsilon_{i,j}} + j\omega\, T_{\chi_{i,j}}(\omega). \tag{14}$$

C. Equivalent Circuit Network of Field Solution

Mathematically, the system (13) is similar to multiport network equations based on admittance matrix representations. Any multiport active network consisting of $N_{\rm P}$ ports [see Fig. 2(a)] can be represented by a series of Norton equivalent circuits. As an example, a portion of the equivalent circuit is shown in Fig. 2(b). The multiport equations in terms of the admittance matrix are obtained by applying Kirchhoff's current law to the ports as

$$[Y_{\rm MN}]\,[V] = -[I_{\rm ps}] \tag{15}$$

where $[V] = [V_1, V_2 \ldots V_{N_{\rm P}}]^T$ is the port voltage vector and $[Y_{\rm MN}]$ is the multiport network admittance matrix [29]. The diagonal coefficient $Y_{{\rm MN}_{k,k}}$ is given by

$$Y_{{\rm MN}_{k,k}} = Y_{0k} + \sum_{\substack{i=1 \\ i\neq k}}^{N_{\rm P}} Y_{k,i}, \qquad k = 1, \ldots, N_{\rm p} \tag{16}$$

where Y_{0k} is the kth port-to-ground admittance and $Y_{k,i}$ the mutual admittance between the kth and ith ports. The off-diagonal coefficients $Y_{{\rm MN}_{i,k}}$ are given by

$$Y_{{\rm MN}ik} = -Y_{i,k}, \qquad i \neq k. \tag{17}$$

Comparing the Whitney element global system (13) and the active multiport network equation (15), the admittances of the Norton equivalent circuits associated with the field equations are given by

$$Y_{0k} = Y_{{\rm WE}_{k,k}}(\omega) - \sum_{\substack{i=1 \\ i\neq k}}^{N_{\rm E}} Y_{{\rm WE}_{k,i}}(\omega) \tag{18a}$$

$$Y_{k,j} = -Y_{{\rm WE}_{{\rm k},j}}(\omega). \tag{18b}$$

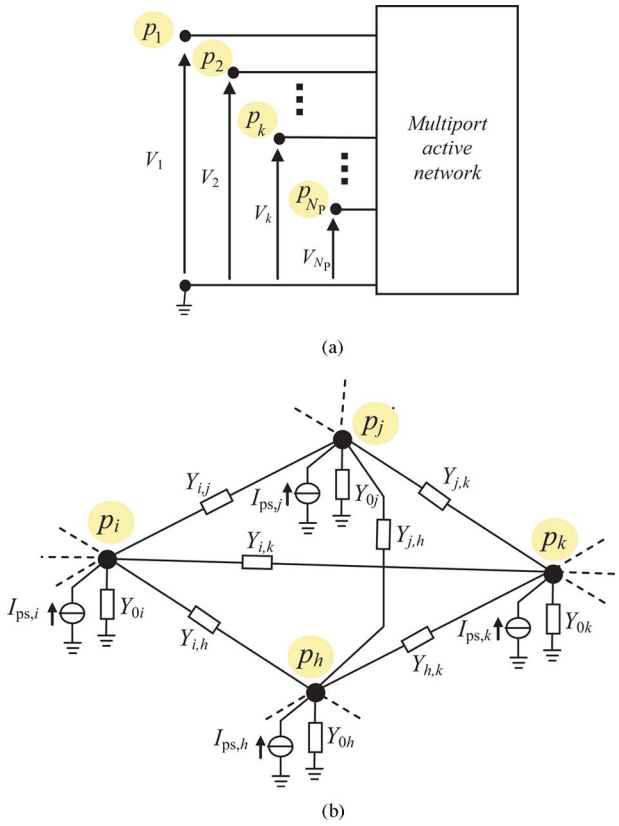

Fig. 2. (a) Multiport network and (b) Norton equivalent circuits corresponding to a portion of the network involving ports i, j, k, and h.

It is worth noting that only a few admittances are present in the Norton equivalent circuits due to the sparse nature of the Whitney element admittance matrix. Consider, for instance, a 2-D case with triangular finite elements. Since every edge is shared by two elements only, five nonzero coefficients per line are present in $[Y_{\rm WE}(\omega)]$. Therefore, only five admittances (i.e., one port-to-ground and four port-to-port admittances) are connected to each port in the corresponding Norton equivalent circuit.

D. SPICE-Like Equivalent Circuit

The admittances (18) appearing in the Norton equivalent circuits are frequency-dependent. To model the network with a SPICE-like circuit simulator, *RLC* models of the network admittances (18) are required. It is worth noting that the coefficients of matrices $[S_\mu]$, $[T_\sigma]$, and $[T_\varepsilon]$ in (11) are constant with frequency, while those of matrix $[T_\chi(w)]$ depend on frequency due to the presence of the frequency-dependent electric susceptibility $\chi(\omega)$ characterizing the dispersive media (see equation (12d)).

With the help of (4) and (14), the mutual admittances (18b) can be rewritten as

$$Y_{i,j}(\omega) = -\frac{S_{\mu_{i,j}}}{j\omega} - T_{\sigma_{i,j}} - j\omega T_{\varepsilon_{i,j}} - j\omega\varepsilon_0 \sum\nolimits_{\rm e} \frac{\varepsilon_{\rm s}^{(\rm e)} - \varepsilon_\infty^{(\rm e)}}{1 + j\omega\tau_0^{(\rm e)}} T_{i,j}^{(\rm e)} \tag{19}$$

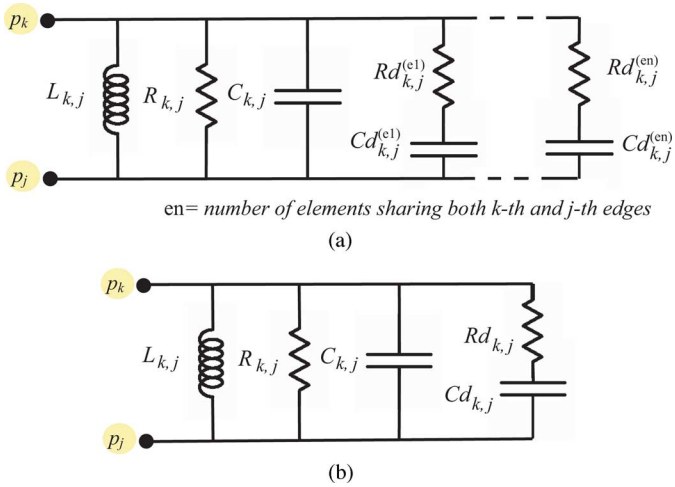

Fig. 3. Equivalent circuit of the mutual admittance $Y_{k,j}(\omega)$ between kth and jth ports: (a) general circuit and (b) simplified circuit in the case of homogeneous dispersive media.

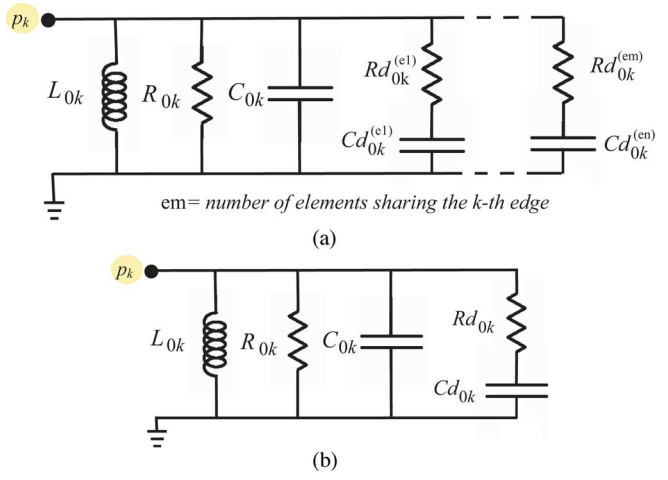

Fig. 4. Equivalent circuit of the port-to-ground admittance $Y_{0k}(\omega)$ at kth port: (a) general circuit and (b) simplified circuit in case of homogeneous dispersive media.

where $\varepsilon_{\rm s}^{(\rm e)}$, $\varepsilon_{\infty}^{(\rm e)}$, and $\tau_0^{(\rm e)}$ are the eth element material constants. The equivalent circuit of the port-to-port admittance is given by the parallel connection of the following branches, as shown in Fig. 3(a):

- inductance $L_{k,j} = -1/S_{\mu_{k,j}}$
- resistance $R_{k,j} = -1/T_{\sigma_{k,j}}$
- capacitance $C_{k,j} = -T_{\varepsilon_{k,j}}$
- and *RC* circuit with

$$Cd_{k,j}^{(\rm e)} = \varepsilon_0(\varepsilon_{\infty}^{(\rm e)} - \varepsilon_{\rm s}^{(\rm e)})T_{k,j}^{(\rm e)}, \qquad {\rm e} = 1, \ldots, {\rm en} \quad (20a)$$

$$Rd_{k,j}^{(\rm e)} = \frac{\tau_0^{(\rm e)}}{Cd_{k,j}^{(\rm e)}}, \qquad {\rm e} = 1, \ldots, {\rm en}. \quad (20b)$$

The number of *RC* branches en is equal to the number of finite elements containing dispersive materials sharing both kth and jth edges. If the elements sharing the two edges are characterized by the same electric susceptibility (i.e., $\varepsilon_s^{(\rm e)} = \varepsilon_s$, $\varepsilon_{\infty}^{(\rm e)} = \varepsilon_{\infty}$, and $\tau_0^{(\rm e)} = \tau_0 \forall {\rm e}$), only one *RC* series branch is necessary, and the circuit reduces to the one shown in Fig. 3(b). In fact, the frequency-dependent term multiplying the mass matrix in (19) can be moved out of the assembly operator, and the series resistance and capacitance are then given by

$$Cd_{k,j} = \varepsilon_0(\varepsilon_{\infty} - \varepsilon_{\rm s})T_{k,j} \quad (21a)$$

$$Rd_{k,j} = \frac{\tau_0}{Cd_{k,j}}. \quad (21b)$$

The equivalent circuit of the kth port-to-ground admittance Y_{0k} is derived from (18a) in a similar way. Adopting the notation of Fig. 4(b), the parameters of the different parallel branches are given by

$$L_{0k} = \left(S_{\mu_{k,k}} + \sum_{\substack{i=1 \\ i \neq k}}^{N_{\rm E}} S_{\mu_{k,i}} \right)^{-1} \quad (22a)$$

$$R_{0k} = \left(T_{\sigma_{k,k}} + \sum_{\substack{i=1 \\ i \neq k}}^{N_{\rm E}} T_{\sigma_{k,i}} \right)^{-1} \quad (22b)$$

$$C_{0k} = T_{\varepsilon_{k,k}} + \sum_{\substack{i=1 \\ i \neq k}}^{N_{\rm E}} T_{\varepsilon_{k,i}} \quad (22c)$$

$$Cd_{0k}^{(\rm e)} = \varepsilon_0(\varepsilon_{\infty}^{(\rm e)} - \varepsilon_{\rm s}^{(\rm e)}) \left(T_{k,k}^{(\rm e)} + \sum_{\substack{i=1 \\ i \neq k}}^{N_{\rm E}} T_{k,i}^{(\rm e)} \right), \quad {\rm e} = 1, \ldots, {\rm em} \quad (22d)$$

$$Rd_{0k}^{(\rm e)} = \frac{\tau_0^{(\rm e)}}{{\rm C}d_{0k}^{(\rm e)}}, \qquad {\rm e} = 1, \ldots, {\rm em} \quad (22e)$$

where em is the number of elements filled by dispersive materials and sharing the kth edge.

In this case also, if the elements sharing the kth edge are characterized by the same electric susceptibility (i.e., $\varepsilon_{\rm s}^{(\rm e)} = \varepsilon_{\rm s}$, $\varepsilon_{\infty}^{(\rm e)} = \varepsilon_{\infty}$, and $\tau_0^{(\rm e)} = \tau_0 \forall {\rm e}$), then just one *RC* branch is necessary with [see Fig. 5(b)]

$$Cd_{0k} = \varepsilon_0(\varepsilon_{\infty} - \varepsilon_{\rm s}) \left(T^{k,k} + \sum_{\substack{i=1 \\ i \neq k}}^{N_{\rm E}} T_{k,i} \right) \quad (23a)$$

$$Rd_{0k} = \frac{\tau_0}{Cd_{0k}}. \quad (23b)$$

III. SPICE-Like Equivalent Circuit for Dispersive Media Described by Multiterm Debye Model

The first-order Debye relation (4) is suitable for modeling media characterized by a single relaxation process. This is often the case for dielectric substrates used in ICs and biological

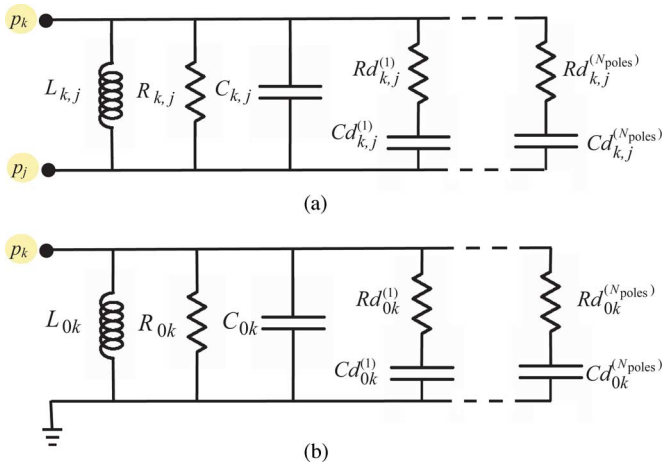

Fig. 5. Simplified equivalent circuits of the admittances (a) $Y_{k,j}(\omega)$ and (b) $Y_{0k}(\omega)$ in case of homogeneous dispersive media.

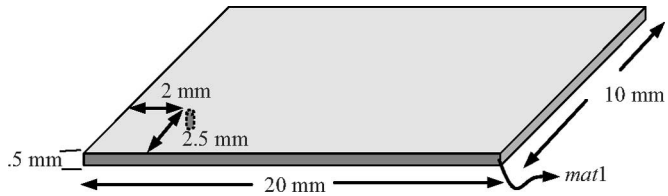

Fig. 6. Geometry of a PCB.

TABLE I
DEBYE MODEL PARAMETERS OF THE MATERIALS

Material type	σ_0 (mS/m)	ε_s	ε_∞	τ_0 (ps)
*mat*1	0	22.670	11.098	32.34
*mat*2	0	4.500	4.500	0
*mat*3	2.531	4.504	4.420	46.37

tissues when attention is focused on a frequency range of about one decade [3], [7].

In diagnostic and therapeutic medical applications and in studies of possible hazards of EM fields, a more accurate model of the dielectric properties of biological tissues is necessary so as to calculate the internal EM fields resulting from exposure to nonionizing fields. Most tissues do not exhibit single, time-constant relaxation behavior, and multiple relaxation processes might occur in parallel, each with a different relaxation time.

When a broadband frequency response is required, it is necessary to describe the behavior of the electric susceptibility in the whole frequency spectrum accurately. In these cases, the following multiterm Debye model can be adopted:

$$\chi(\omega) = \sum_{h=1}^{N\text{poles}} \frac{\varepsilon_{sh} - \varepsilon_\infty}{1 + j\omega\tau_h} \tag{24}$$

where N_{poles} is the number of poles, ε_{sh} the hth static permittivity, and τ_h the hth relaxation time. For any given number of poles, the optimal values of ε_{sh} and τ_h in (24) can be obtained by fitting this response to the measured relative permittivity and conductivity [27].

The Whitney element formulation proposed in Section II-B can be easily extended to accommodate the multiterm Debye model, and the corresponding SPICE-like equivalent circuit is derived in a straightforward manner. In fact, every term of the expansion (24) can be modeled by an *RC* branch as described in the previous section. In the case of a homogeneous dispersive medium, the equivalent circuits of the admittances $Y_{k,j}$ and Y_{0k} are shown in Fig. 5.

The multiterm Debye function expansion is suitable for modeling the dielectric behavior of most physical materials. Moreover, because of the causal nature of physical materials, the real and imaginary parts of the permittivity are related to each other via the Kramers–Kronig relation [4], and a simplified fitting procedure can be used to approximate empirical complex permittivity [27].

IV. NUMERICAL RESULTS

The formulation presented here was validated by modeling three simple geometries. The first geometry is the rectangular printed circuit board (PCB) structure shown in Fig. 6. The structure is composed of two metal planes and a dielectric substrate. The size of the planes was 20 mm $\times$10 mm. They were modeled as perfect electric conductors (PECs). The dielectric substrate between the two planes had a thickness of 0.5 mm. The fringing field was neglected and the four side walls of the board were modeled as perfect magnetic conductors (PMCs). The dielectric material was named *mat*1. The first-order Debye model parameters of *mat*1 are shown in Table I and the relative permittivity and conductivity versus frequency are shown in Fig. 7. The board was excited by an ideal current source located near the corner, 2 and 2.5 mm from the edges, as shown in Fig. 6.

The FEM matrix was calculated for this structure and the matrix equation was solved directly to obtain the real and imaginary parts of the input impedance shown in Fig. 8 by small crosses. The corresponding SPICE circuit was then generated from the FEM matrix and the problem was simulated using HSPICE [30]. The result of the HSPICE circuit simulation is indicated by the solid curve in Fig. 8. The figure shows the results from 100 MHz to 100 GHz. The dielectric property of the material changes significantly from 2 to 20 GHz and many resonant peaks occur at frequencies above 50 GHz. In this example, the values of all the capacitors were on the order of 10^{-20}, while the inductor values were on the order of 10^{-5}. To improve the numerical accuracy of the simulation, all the capacitance values and source currents were increased by a factor of 10^3, and the inductances and resistances were decreased by a factor of 10^3, yielding the same output voltage.

Fig. 9 shows the geometry of another PCB structure. In this example, the planes have the same size as the planes in the first example. The dielectric substrate, however, is composed of two equal-sized pieces touching each other. One of them is *mat*1, the other is *mat*2, which is lossless and has a constant permittivity, as indicated in Table I. The current source is located in the *mat*2 part of the board.

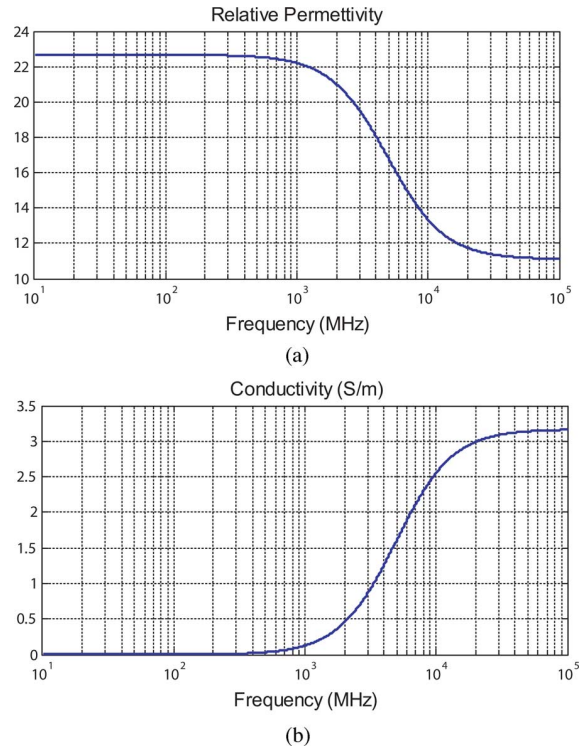

Fig. 7. Relative permittivity and conductivity versus frequency for a Debye material *mat*1.

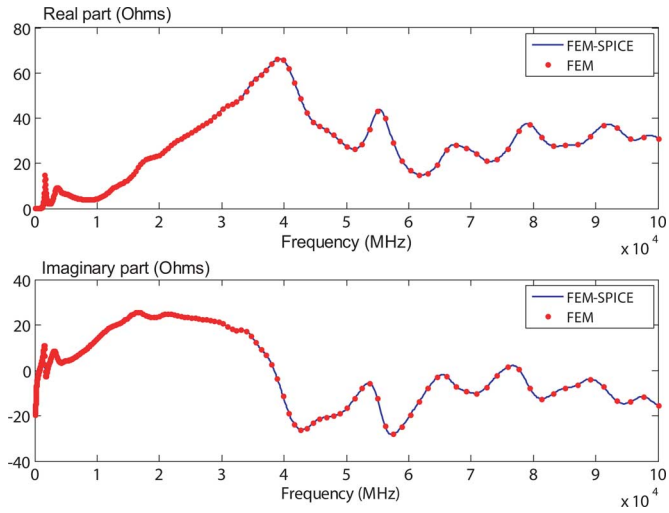

Fig. 8. Input impedance of the first PCB.

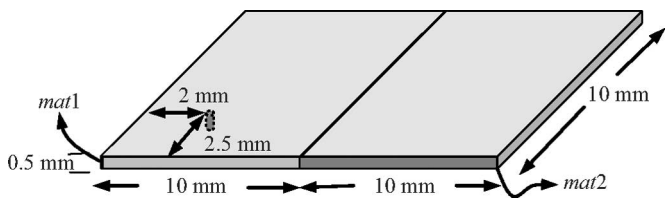

Fig. 9. Geometry of the PCB with two materials.

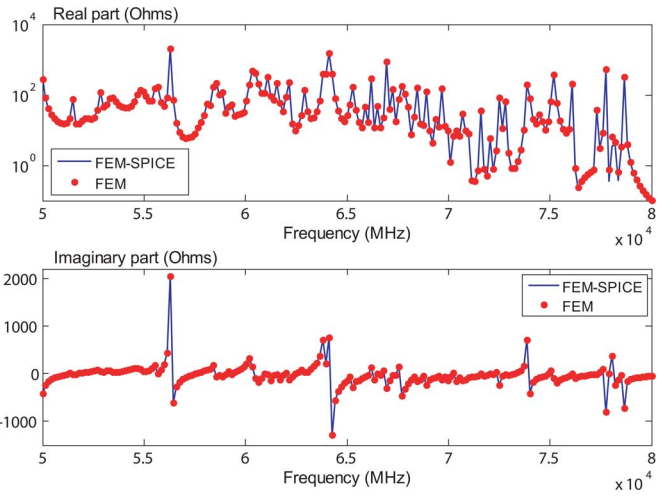

Fig. 10. Input impedance of the PCB with two materials.

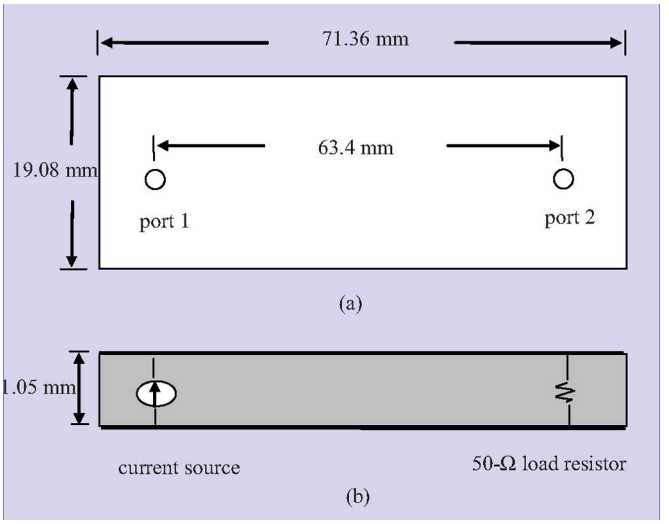

Fig. 11. Geometry of the parallel plate transmission line. (a) Top view. (b) Side view.

The calculated input impedance of the second structure is shown in Fig. 10. The results of the two methods match very well from 100 MHz to 100 GHz. For a better view of the peaks, the figure also shows the results from 50 to 80 GHz with the y-axis of the real part changed to log scale.

The third example is a parallel plate transmission line with a lossy dielectric and lumped-element terminations (see Fig. 11). The dimensions of the plates are 71.36 mm $\times$19.08 mm. The thickness of the dielectric between the plates is 1.05 mm. The dielectric material is *mat*3 as defined in Table I. A 50-Ω source is located near one end of the line and a 50-Ω load resistor is located 63.4 mm away near the other end of the line.

Fig. 12 shows the real and imaginary parts of the voltage calculated at the source port from 500 MHz to 5 GHz, where the dielectric constant varies the most with frequency. It is worth noting that when incorporating lumped components, the values of these components in the SPICE circuit are related to the size

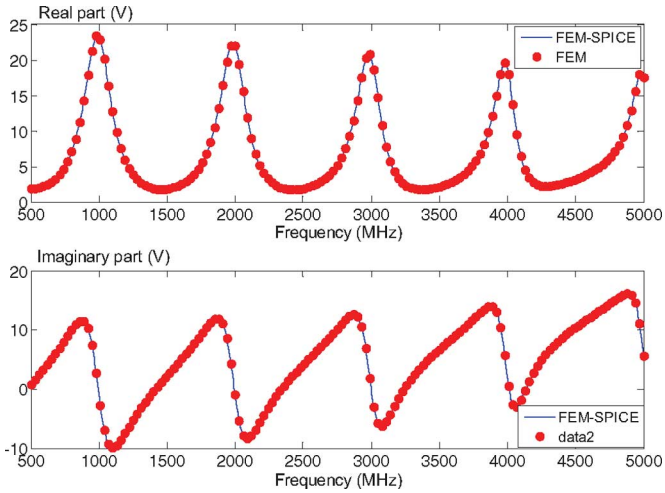

Fig. 12. Voltage at the source end of the transmission line in the third example.

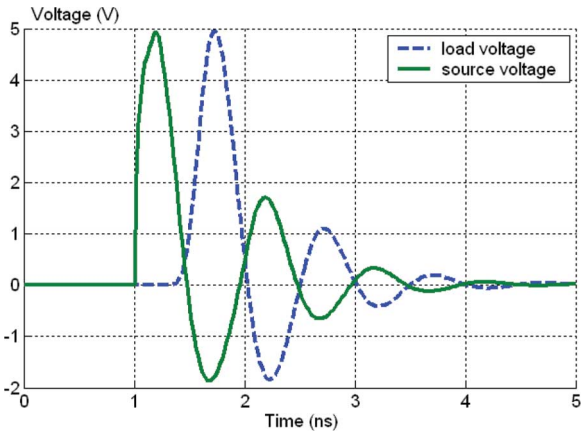

Fig. 13. Voltage at the source and load ends of a parallel plate transmission line excited by a dumped sinusoidal waveform.

of the FEM mesh. In some cases, this can result in unrealistic component values.

Finally, a time-domain simulation of the parallel plate transmission line structure shown in Fig. 11 was performed. The current source waveform was a decaying sinusoid at a frequency of 1 GHz with a peak value of 1 A. The wave had a time delay of 1 ns and a damping factor of 2×10^9. The source waveform expression was

$$i(t) = e^{2(1-t)} \sin(2\pi(t-1)), \qquad t > 1$$

where the time t is in nanoseconds. The parallel-plate transmission line was terminated at port 2 by a 12-Ω characteristic impedance.

The voltage waveforms at the source and load are shown in Fig. 13 by dashed and solid lines, respectively. As expected, the voltage at the load is a delayed copy of the voltage at the source.

V. Conclusion

A circuit-oriented FEM formulation has been proposed that supports the modeling of frequency-dispersive materials. This approach generates Norton equivalent circuits based on the finite-element formulation in the field domain. The paper describes how first-order Debye materials are characterized by *RC* series branches and how this approach can be extended to model more complicated materials. Three sample structures were analyzed using this technique. The examples demonstrate that this approach is capable of modeling structures with mixed dispersive materials. The proposed FEM-SPICE method is a potentially powerful tool for analyzing field-circuit coupled problems due to its ability to exploit the advanced capabilities of SPICE-like simulators for modeling linear/nonlinear components embedded in distributed EM geometries.

References

[1] C. Polk and E. Postow, *Handbook of Biological Effects of Electromagnetic Fields*, 2nd ed. Boca Raton, FL: CRC Press, 1996.
[2] O. P. Gandhi, *Biological Effects and Medical Applications of Electromagnetic Energy*. Englewood Cliffs, NJ: Prentice-Hall, 1990.
[3] K. C. Gupta, R. Garg, I. Bahl, and P. Bhartia, *Microstrip Lines and Slotlines*, 2nd ed. Boston, MA: Artech House, 1996.
[4] S. Ramo, J. R. Whinnery, and T. Van Duzer, *Fields and Waves in Communication Electronics*, 3rd ed. New York: Wiley, 1994.
[5] N. Marcuvitz, *Waveguide Handbook*. (IEE Electromagnetic Waves Series 21). Herts, U.K.: IET, 1986.
[6] R. J. Luebbers, F. Hunsberg, and K. S. Kunz, "A frequency-dependent finite-difference time-domain formulation for dispersive materials," *IEEE Trans. Electromagn. Compat.*, vol. 32, no. 3, pp. 222–227, Aug. 1990.
[7] D. M. Sullivan, "A frequency dependent FDTD method for biological application," *IEEE Trans. Microw. Theory Tech.*, vol. 40, no. 3, pp. 532–539, Mar. 1992.
[8] R. J. Luebbers and F. Hunsberg, "FDTD for Nth order dispersive media," *IEEE Trans. Antennas Propag.*, vol. 40, no. 11, pp. 1297–1301, Nov. 1992.
[9] D. F. Kelley and R. J. Luebbers, "Piecewise linear recursive convolution for dispersive media using FDTD," *IEEE Trans. Antennas Propag.*, vol. 44, no. 6, pp. 792–797, Jun. 1996.
[10] J. F. Lee, "Whitney elements time domain (WETD) method," *IEEE Trans. Magn.*, vol. 31, no. 3, pp. 1325–1329, May 1995.
[11] F. Maradei, "A frequency-dependent WETD formulation for dispersive materials," *IEEE Trans. Magn.*, vol. 37, no. 5, pp. 3303–3306, Sep. 2001.
[12] D. Jiao and J. M. Jin, "Time-domain finite-element modeling of dispersive media," *IEEE Microw. Wireless Compon. Lett.*, vol. 11, no. 5, pp. 220–222, May 2001.
[13] W. Sui, D. A. Christensen, and C. H. Durney, "Extending the two-dimensional FDTD method to hybrid electromagnetic systems with active and passive lumped elements," *IEEE Trans. Microw. Theory Tech.*, vol. 19, no. 12, pp. 4724–730, Apr. 1992.
[14] Y. S. Tsuei, A. C. Cangellaris, and J. L. Prince, "Rigorous electromagnetic modeling of the chip-to-package (first level) interconnections," *IEEE Trans. Comp., Hybrids, Manuf. Technol.*, vol. 16, no. 8, pp. 876–883, Dec. 1993.
[15] R. J. Luebbers, J. Beggs, and K. Chamberlain, "Finite difference time-domain calculation of transients in antennas with nonlinear loads," *IEEE Trans. Antennas Propag.*, vol. 41, no. 5, pp. 566–573, May 1993.
[16] M. Al-Asadi, T. M. Benson, and C. Christopoulos, "Interfacing field problems modelled by TLM to lumped circuits," *Inst. Electr. Eng. Electron. Lett.*, vol. 30, no. 4, pp. 290–291, Feb. 1994.
[17] M. Piket-May, A. Taflove, and J. Baron, "FD-TD modeling of digital signal propagation in 3D circuits with passive and active loads," *IEEE Trans. Microw. Theory Tech.*, vol. 42, no. 8, pp. 1514–1523, Aug. 1994.
[18] C. N. Kuo, B. Houshmand, and T. Itoh, "Full-wave analysis of packaged microwave circuits with active and non-linear devices: An FDTD approach," *IEEE Trans Microw. Theory Tech.*, vol. 45, no. 5, pp. 819–826, May 1997.
[19] W. Pinello, A. Ruehli, and A. Cangellaris, "Analysis of interconnect and package structures using PEEC models with radiated emissions," in *Proc. IEEE 1997 Int. Symp. Electromagn*, Austin, TX,, Aug. 18–22, 1997, pp. 353–358.
[20] K. Guillord, M. F. Wong, V. F. Hanna, and J. Citerne, "New global finite element analysis of microwave circuits including lumped elements," *IEEE Trans. Microw. Theory Tech.*, vol. 44, no. 12/2, pp. 2587–2594, Dec. 1996.

[21] M. Feliziani and F. Maradei, "Modeling of electromagnetic fields and electrical circuits with lumped and distributed elements by the WETD method," *IEEE Trans. Magn.*, vol. 35, no. 3, pp. 1666–1669, May 1999.
[22] K. Guillord, M.-F. Wong, V. F. Hanna, and J. Citerne, "A new global time-domain electromagnetic simulator of microwave circuits including lumped elements based on finite-element method," *IEEE Trans Microw. Theory Tech.*, vol. 47, no. 10, pp. 2045–2048, Oct. 1999.
[23] S. H. Chang, R. Coccioli, Y. Qian, and T. Itoh, "A global finite-element time domain analysis of active nonlinear microwave circuits," *IEEE Trans. Microw. Theory Tech.*, vol. 47, no. 12, pp. 2410–2416, Dec. 1999.
[24] M. Feliziani and F. Maradei, "FEM solution of time-harmonic electromagnetic fields by an equivalent electrical network," *IEEE Trans. Magn.*, vol. 34, no. 3, pp. 1666–1669, Jul. 2000.
[25] M. Feliziani and F. Maradei, "Circuit-oriented FEM: solution of circuit-field coupled problems by circuit equations," *IEEE Trans. Magn.*, vol. 38, no. 2, pp. 965–968, Mar. 2002.
[26] C. Guo and T. H. Hubing, "Circuit models for power bus structures on printed circuit boards using a hybrid FEM-SPICE method," *IEEE Trans. Adv. Packag.*, vol. 29, no. 3, pp. 441–447, Aug. 2006.
[27] D. F. Kelly and R. J. Luebbers, "Debye function expansions of empirical models of complex permittivity for use in FDTD solutions," in *Proc. 2003 Antennas Propag. Int. Symp.*, pp. 372–375.
[28] J. Jin, *The Finite Element Method in Electromagnetics*, 2nd ed. New York: Wiley, 2002.
[29] D. Pozar, *Microwave Engineering*, 2nd ed. New York: Wiley, 1998.
[30] HSPICE ver. 2007.09, Synopsis, Inc. Mountain View, CA.

Francescaromana Maradei (M'94–SM'06) received the Laurea (*cum laude*) and Ph.D. degree in electrical engineering from Sapienza University, Rome, Italy, in 1992 and 1997, respectively, and the Diplome d'Etudes Approfondies (DEA) in electrical engineering from the Institut National Polytechnique de Grenoble, Laboratoire d'Electrotechnique de Grenoble, Grenoble, France, in 1993.

In 1996, she joined the Department of Electrical Engineering, Sapienza University, where she is currently an Associate Professor. Her current research interests include numerical techniques and their application to electromagnetic compatibility (EMC) problems (shielding and transmission line analysis).

Dr. Maradei received the James Melcher Price Paper Award for the paper "Analysis of upset and failures due to ESD by the FDTD-INBCs method," the Oral Presentation Best Paper Award at the International Symposium on Electromagnetic Compatibility-–EMC ROMA 1994, Rome, Italy, and the Poster Presentation Best Paper Award at the International Symposium on Electromagnetic Compatibility-–EMC EUROPE 2000, Brugge, Belgium. She is a member of the Board of Directors of the IEEE Electromagnetic Compatibility Society, where she is also serving as a Chapter Coordinator. From 1999 to 2000, she was an Associate Editor of the IEEE TRANSACTIONS ON ELECTROMAGNETIC COMPATIBILITY. Since 1998, she has been a member of the Editorial Board of the IEEE Conference on Electromagnetic Field Computation (CEFC) and the IEEE COMPUMAG Conference.

Haixin Ke (M'06) received the B.S. and M.S. degrees from Tsinghua University, Beijing, China, in 1998 and 2001, respectively, and the Ph.D. degree from the University of Missouri, Rolla, in 2006, all in electrical engineering.

He is currently a Postdoctoral Researcher at Clemson University, Clemson, SC. His current research interests include computational electromagnetics, electromagnetic compatibility, and vehicular electronic systems.

Todd H. Hubing (S'82–M'82–SM'93–F'06) received the B.S. degree from the Massachusetts Institute of Technology, Boston, in 1980, the M.S. degree from Purdue University, West Lafayette, IN, in 1982, and the Ph.D. degree from North Carolina State University, Raleigh, in 1988, all in electrical engineering.

From 1982 to 1989, he was with the Electromagnetic Compatibility Laboratory, IBM Communications Products Division, Research Triangle Park, NC. In 1989, he joined the faculty at the University of Missouri, Rolla (UMR), where he worked with faculty and students to analyze and develop solutions for a wide range of electromagnetic compatibility (EMC) problems affecting the electronics industry. In 2006, he joined Clemson University, Clemson, SC, as the Michelin Professor for Vehicular Electronics, and is engaged in EMC and computational electromagnetic modeling, particularly as it is applied to automotive and aerospace electronic designs. He was an Associate Editor of the *Journal of the Applied Computational Electromagnetics Society.*

Prof. Hubing was an Associate Editor of the IEEE TRANSACTIONS ON ELECTROMAGNETIC COMPATIBILITY and the IEEE EMC SOCIETY NEWSLETTER. He was a member of the Board of Directors for both the Applied Computational Electromagnetics Society and the IEEE EMC Society. From 2002 to 2003, he was the President of the IEEE EMC Society.